ORIGINAL RESEARCH

# Efficacy of Novel Highly Specific Bromodomain-Containing Protein 4 Inhibitors in Innate Inflammation–Driven Airway Remodeling

Bing Tian[1,2], Zhiqing Liu[3], Julia Litvinov[1], Rosario Maroto[1], Mohammad Jamaluddin[4], Erik Rytting[5], Igor Patrikeev[6], Lorenzo Ochoa[6], Gracie Vargas[6], Massoud Motamedi[6], Bill T. Ameredes[1,2,3,4,7], Jia Zhou[2,3], and Allan R. Brasier[8]

[1]Department of Internal Medicine, [2]Sealy Center for Molecular Medicine, [3]Department of Pharmacology and Toxicology, [4]Institute for Translational Sciences, [5]Department of Obstetrics and Gynecology, [6]The Center for Biomedical Engineering, and [7]Sealy Center for Environmental Health and Medicine, University of Texas Medical Branch, Galveston, Texas; and [8]School of Medicine and Public Health, University of Wisconsin–Madison, Madison, Wisconsin

ORCID ID: 0000-0002-5012-4090 (A.R.B.).

## Abstract

NF-κB/RelA triggers innate inflammation by binding to bromodomain-containing protein 4 (BRD4), an atypical histone acetyltransferase (HAT). Although RelA·BRD4 HAT mediates acute neutrophilic inflammation, its role in chronic and functional airway remodeling is not known. We observed that BRD4 is required for Toll-like receptor 3 (TLR3)-mediated mesenchymal transition, a cell-state change that is characteristic of remodeling. We therefore tested two novel highly selective BRD4 inhibitors, ZL0420 and ZL0454, for their effects on chronic airway remodeling produced by repetitive TLR3 agonist challenges, and compared their efficacy with that of two nonselective bromodomain and extraterminal (BET) protein inhibitors, JQ1 and RVX208. We observed that ZL0420 and ZL0454 more potently reduced polyinosinic:polycytidylic acid–induced weight loss and fibrosis as assessed by microcomputed tomography and second harmonic generation microscopy. These measures correlated with the collagen deposition observed in histopathology. Importantly, the ZL inhibitors were more effective than the nonselective BET inhibitors at equivalent doses. The ZL inhibitors had significant effects on lung physiology, reversing TLR3-associated airway hyperresponsiveness and increasing lung compliance *in vivo*. At the molecular level, ZL inhibitors reduced elaboration of the transforming growth factor-β–induced growth program, thereby preventing mucosal mesenchymal transition and disrupting BRD4 HAT activity and complex formation with RelA. We also observed that ZL0454 treatment blocked polyinosinic:polycytidylic acid–associated expansion of the α-SMA1$^+$/COL1A$^+$ myofibroblast population and prevented myofibroblast transition in a coculture system. We conclude that *1*) BRD4 is a central effector of the mesenchymal transition that results in paracrine activation of myofibroblasts, mechanistically linking innate inflammation to airway hyperresponsiveness and fibrosis, and *2*) highly selective BRD4 inhibitors may be effective in reversing the effects of repetitive airway viral infections on innate inflammation–mediated remodeling.

**Keywords:** airway remodeling; epithelial–mesenchymal transition; lung optical clearing; multiphoton microscopy

### Clinical Relevance

This work demonstrates the activation of the NF-κB–bromodomain-containing protein 4 pathway and validates this pathway as a therapeutic target to block airway remodeling in chronic lung disease.

(Received in original form December 29, 2017; accepted in final form July 23, 2018)

Supported by the Sealy Center for Molecular Medicine, Sealy Center for Environmental Health and Medicine, Signaling in Airway Inflammation/National Institute of Allergy and Infectious Diseases grant PO1 AI068865 (A.R.B.), University of Texas Medical Branch Clinical and Translational Science Award UL1TR000071 (A.R.B.), National Institute of Environmental Health Sciences grants P30 ES006676 (A.R.B., B.T., and B.T.A.) and T32ES007254 (B.T.A. and J.L.), the Brown Foundation (B.T.A.), the University of Texas Medical Branch Technology Commercialization Program (A.R.B., B.T., J.Z., and E.R.), Sanofi Innovation Awards (iAwards) (A.R.B., B.T., J.Z., and E.R.), and National Science Foundation grant DMS-1361411/DMS-1361318 (A.R.B.).

Author Contributions: Conception and design: B.T., Z.L., J.L., R.M., M.J., I.P., G.V., M.M., B.T.A., J.Z., and A.R.B. Analysis and interpretation: B.T., J.L., R.M., M.J., E.R., I.P., L.O., G.V., M.M., B.T.A., J.Z., and A.R.B. Writing of the manuscript: B.T., J.L., R.M., E.R., M.M., B.T.A., J.Z., and A.R.B.

Correspondence and requests for reprints should be addressed to Allan R. Brasier, M.D., Institute for Clinical and Translational Research, University of Wisconsin-Madison School of Medicine and Public Health, 4246 Health Sciences Learning Center, 750 Highland Avenue, Madison, WI 53705. E-mail: abrasier@wisc.edu.

This article has a data supplement, which is accessible from this issue's table of contents at www.atsjournals.org.

Am J Respir Cell Mol Biol Vol 60, Iss 1, pp 68–83, Jan 2019

Originally Published in Press as DOI: 10.1165/rcmb.2017-0445OC on August 28, 2018
Internet address: www.atsjournals.org

Over 300 million adults and children suffer from asthma worldwide, making this disease a significant public health problem (1). Asthma is a chronic inflammatory disorder of the airways whose clinical course is characterized by intermittent episodic exacerbations involving increased inflammation, bronchoconstriction, and airway obstruction that can require urgent medical intervention (2). Epidemiological studies have shown that acute respiratory viral infections cause up to one-half to two-thirds of asthma exacerbations (3). Apart from acute morbidity from exacerbations, large-scale observational studies have demonstrated that individuals with asthma can exhibit a more rapid age-related decline in pulmonary capacity (4, 5), and this process is accelerated by frequent exacerbations (6–10). In fact, an accelerated decline in lung function due to frequent exacerbations is also characteristic of patients with fixed airway obstruction (11). Because current therapies are effective in treating allergic inflammation but do not reverse structural remodeling (12), an understanding of the pathways that link acute inflammatory exacerbations to airway remodeling is urgently needed, as highlighted by the Expert ATS Panel on airway remodeling (13).

Airway remodeling is a constellation of structural changes in the airway, including epithelial injury, disruption of the epithelial barrier function, subepithelial collagen deposition in the lamina reticularis, myofibroblast hyperplasia, and smooth muscle hypertrophy linked with airway hyperresponsiveness (AHR) (9, 14, 15). Although airway remodeling is a complex phenomenon that is influenced by allergic inflammation, increasing evidence suggests that the epithelial injury–repair response also plays an important role (12, 16). Upon injury, epithelial cells secrete fibrogenic cytokines, including IL-6 and transforming growth factor β (TGF-β), that trigger myofibroblast transdifferentiation and secretion of extracellular matrix (ECM) proteins such as collagen (COL) and fibronectin 1 (FN1). Using a model of repetitive inflammation induced by viral pattern activation of the epithelial Toll-like receptor 3 (TLR3) pathway, we recently identified a molecular link among innate inflammation, mucosal cell state transition, and airway fibrosis (17, 18). TLR3 activates epithelial NF-κB/RelA signaling in the proximal and small airways, acutely producing neutrophilic chemokines and inflammation, but chronic exposure triggers epithelial–mesenchymal transition (EMT) and interstitial collagen deposition (19). These mesenchymal cell state changes are due to coordinated, global epigenetic reprogramming of over 3,000 genes mediated by histone acetyltransferases (HATs) (18). However, the mechanisms by which acute inflammation leads to epigenetic reprogramming and airway remodeling are incompletely understood.

An important insight into how innate inflammation affects gene programs was provided by the discovery that RelA forms a complex with bromodomain-containing protein 4 (BRD4) in airway mucosa in response to respiratory viral infection, cytokine stimulation, TLR3 signaling, and TGF-β activation (20–26). BRD4 is an acetylated histone reader with HAT activity that is responsible for acetylation of histone H3 on Lys residue 122 (H3K122Ac), a posttranslational modification that destabilizes nucleosome structure (25). Importantly, we have found that BRD4 HAT activity is inducible and dependent on binding activated RelA (21–23).

Using structure-guided drug design, we recently developed two highly selective small-molecule inhibitors specific for the BRD4 isoform (23). Accordingly, in the present study, we used these medicinal chemistry probes to examine the role of BRD4 in TLR3-induced airway remodeling *in vivo*, using a mouse model developed to replicate recurrent virus-induced asthma exacerbations. Our findings indicate that mucosal BRD4 is required for mesenchymal transition and the production of paracrine factors that are important for myofibroblast transdifferentiation and airway fibrosis. The results obtained from administration of our highly selective novel BRD4 inhibitors indicate that they are nontoxic and effective in reversing the effects of repetitive airway viral infections on innate inflammation–mediated airway remodeling. These novel compounds may represent a promising set of compounds for potential therapeutic development.

## Methods

Details regarding the materials and methods used in this work are available in the data supplement.

## Results

### BRD4 Is Required for TLR3-initiated Mesenchymal Transition

We previously demonstrated that TLR3-induced innate signaling triggered mesenchymal transition of primary human small airway epithelial cells (hSAECs) in an NF-κB/RelA-dependent manner (27). To determine whether this process requires BRD4, we first examined the effect of BRD4 silencing using siRNA-mediated transfection. BRD4 siRNA produced a >80% inhibition of basal *BRD4* mRNA levels (Figure 1A). Although polyinosinic: polycytidylic acid (poly[I:C]) induced a twofold increase in steady-state *BRD4* mRNA levels, BRD4 siRNA similarly silenced *BRD4* expression in the mesenchymal state. We next evaluated the effect of BRD4 silencing on the core mesenchymal regulators. BRD4 depletion reduced the 13.8-fold increase in *SNAI1* mRNA in control transfectants to 4.6-fold in BRD4 siRNA-transfected cells ($P < 0.05$). Similarly the 5.7-fold increase in *ZEB1* mRNA was reduced to 2.1-fold (Figure 1A). Correspondingly, BRD4 depletion inhibited poly(I:C)-induced expression of the mesenchymal intermediate filament protein *VIM* mRNA, messages for the ECM-modifying gene program, including *FN1*, *COL1A*, and *MMP9* mRNAs, as well as autocrine growth factor *IL6* mRNA (Figure 1A). Collectively these data indicate that the TLR3-induced mesenchymal program requires BRD4 expression.

We recently synthesized two chemically distinct, highly selective BRD4 inhibitors that show a 30-fold greater selectivity for binding the BRD4 bromodomains (BDs) than the closely related BRD2 isoform (23), and greater cellular potency than the prototypical inhibitors JQ1 and RVX208 (23). To determine whether these inhibitors affected the poly(I:C)-induced mesenchymal transition in a manner similar to that of BRD4 siRNA depletion, we tested the effect of ZL0454 on the poly(I:C)-induced mesenchymal program in hSAECs. ZL0454 treatment significantly reversed the effect of tonic poly(I:C) on the downregulation of epithelial cadherin (*CDH1*) mRNA and reduced the 17-fold induction of *SNAI1* mRNA to less than threefold, and the 8.6-fold induction of *ZEB1* mRNA to less than twofold (Figure 1B). Similarly, the 56-fold

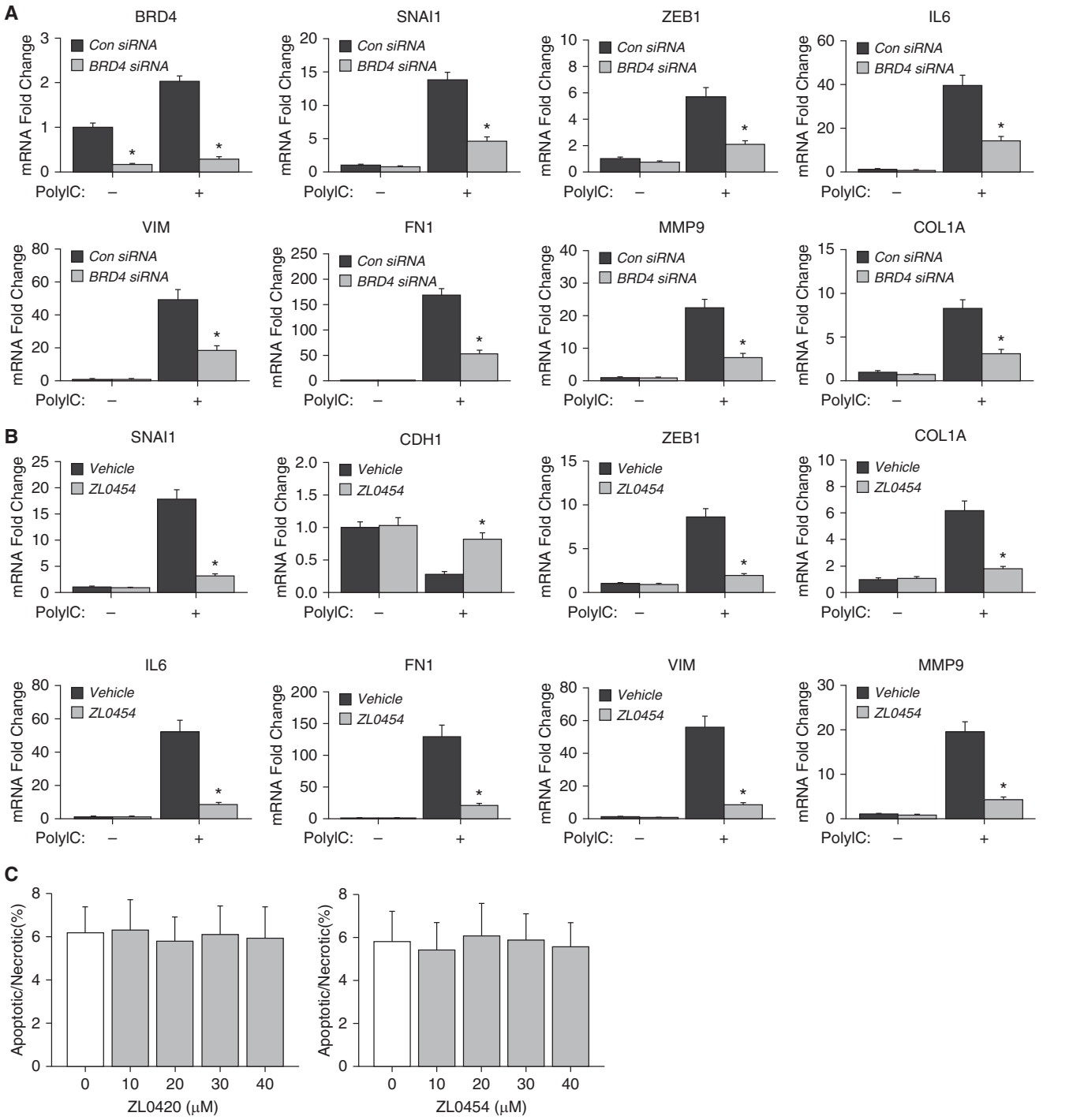


**Figure 1.** Bromodomain-containing protein 4 (BRD4) mediates Toll-like receptor 3 (TLR3)-induced mesenchymal transition in human small airway epithelial cells (hSAECs). (*A*) Effect of BRD4 depletion. hSAECs were left untreated or stimulated with polyinosinic:polycytidylic acid (poly[I:C]; 10 μg/ml) for 15 days in the absence or presence of BRD4 depletion by siRNA-mediated transfection. Shown are qRT-PCR assays for *BRD4* mRNA itself; the mesenchymal regulators *SNAI1* and *ZEB1;* the extracellular matrix (ECM)-modifying genes *COL1A*, *FN1*, *MMP9*, and *VIM*; and autocrine growth factor *IL6* mRNAs. Data are presented as fold-change mRNA abundance normalized to *PPIA* (cyclophilin A). *$P < 0.01$, $n = 3$. (*B*) Effect of a selective BRD4 inhibitor. hSAECs were untreated or stimulated with poly(I:C) (PolyIC) for 15 days in the absence or presence of the selective BRD4 inhibitor ZL0454. Shown is the fold change in normalized mRNA expression for mesenchymal regulators, the epithelial marker *CDH1* (E-cadherin), ECM-modifying proteins, and *IL6*. (*C*) Toxicity assessment of selective BRD4 inhibitors. hSAECs were incubated with the selective BRD4 inhibitors ZL0420 and ZL0454 overnight at a final concentration of 0, 10, 20, 30, and 40 μM, respectively. The treated cells were collected, followed by flow-cytometric detection of apoptosis/necrosis by Annexin V/PE staining. Data are presented as the total percentage of cells in apoptosis and necrosis; $n = 3$. COL1A = collagen 1A; Con = control; FN1 = fibronectin; MMP9 = matrix metalloproteinase 9; SNAI = Snail family transcription factor; VIM = vimentin; ZEB = Zinc finger E-box-binding protein.

increase of *VIM*, the 6.2-fold increase of *COL1A*, the 129-fold increase of *FN1*, the 19.5-fold induction of *MMP9*, and the 52-fold induction of *IL6* mRNAs were reduced to 8.6-fold, 1.8-fold, 20.4-fold, 4.3-fold, and 8.5-fold, respectively ($P < 0.05$, ANOVA; Figure 1B). We conclude that the BRD4 inhibitors produced inhibition of the mesenchymal transition similar to that achieved with BRD4 depletion. Similar effects of ZL0420 were observed (not shown).

To identify any potential cytotoxic effects of our selective BRD4 inhibitors, we incubated hSAECs with ZL0420 or ZL0454 overnight at a final concentration of 0, 10, 20, 30, or 40 μM. The treated cells were collected, followed by flow-cytometric detection of apoptosis/necrosis via Annexin V/PE staining. No apparent increase in cell death was detected in hSAECs treated with ZL0420 or ZL0454 up to a concentration of 40 μM (Figure 1C). These data indicate that our selective BRD4 inhibitors have no apparent cytotoxic effect.

To confirm that the inhibition of the mesenchymal gene-expression program was functionally significant, we examined the effect of the ZL BRD4 inhibitors on changes in epithelial morphology by fluorescence microscopy. The poly(I:C)-induced increase in actin stress-fiber formation was blocked by treatment with either ZL0420 or ZL0454 (Figures 2A and 2C). Poly(I:C) induced a 9.2-fold increase in the nuclear abundance of H3K122 acetylation, a selective marker of BRD4 HAT activity (21–23, 25). This epigenetic modification was reduced to nearly baseline by treatment with either ZL0420 or ZL0454 (Figures 2A and 2C). By contrast, poly(I:C) had no effect on the global abundance of H3K14 acetylation (Figures 2A and 2C), a BRD4-independent histone marker (25). Importantly, H3K14Ac abundance was unaffected by either ZL inhibitor (Figures 2A and 2C). In a manner similar to that of H3K122Ac, the 7.2-fold increase in SNAI1 and 12.6-fold increase in VIM fluorescence were reduced to 1.6- and 2-fold by ZL0420 and ZL0454 treatment, respectively (Figures 2B and 2C). Finally, the 80% inhibition of CDH1 by poly(I:C) was attenuated to ~15% by the BRD4 inhibitors (Figures 2B and 2C). These data indicate that the selective BRD4 inhibitors were highly effective in reducing the effects of chronic poly(I:C) on selective BRD4-induced chromatin markers, mesenchymal transition, and ECM remodeling.

### *In Vivo* Efficacy of BRD4 Inhibitors in TLR3-induced Airway Remodeling

***Tissue toxicological assessments.*** Previously, we observed that the mesenchymal transition was associated with airway remodeling in response to chronic TLR3 activation (27). To evaluate the role of BRD4 HAT in this process, we sought to interfere with BRD4 HAT using selective small-molecule inhibitors that we recently developed (23). To exclude the possibility that BRD4 inhibitors have systemic effects, we first evaluated whether escalating doses of ZL0454 had chronic toxicity in mice over 1 month of treatment. We observed that daily administration of parenteral ZL0454 (1–50 mg/kg) had no significant effects on body weight, hematological measures (white blood cells, red blood cells, and platelets), liver function (albumin, globulin, alkaline phosphatase, and alanine aminotransferase), or renal function (creatinine and blood urea nitrogen) (Figure E1 in the data supplement). Moreover, ZL0454 had no discernible effects on hepatic or renal histology, as assessed by hematoxylin and eosin staining of organ tissue slices (not shown), which is consistent with the lack of cytotoxic effects noted above. Collectively, the lack of measurable toxicity at several levels of assessment indicated that our selective BRD4 inhibitor was well tolerated *in vivo*.

***Efficacy assessments.*** We previously established a standardized mouse model of TLR3-induced mesenchymal transition and interstitial fibrosis designed to replicate frequent viral exacerbations (27). In this model, airway remodeling was induced after repetitive intranasal challenges of the TLR3 agonist poly(I:C). We compared the efficacy of equivalent doses of the highly selective BRD4 inhibitors ZL0420 and ZL0454 with the prototypical nonselective bromodomain and extraterminal (BET) protein inhibitors JQ1 and RVX208 in this model (28, 29) (Figure E2). The repetitive administration of poly(I:C) alone (vehicle-treated mice) induced a 20% reduction in body weight, an effect that was normalized by treatment with ZL0454 and ZL0420 inhibitors (Figure 3A). By contrast, mice treated with JQ1 showed an intermediate weight loss compared with poly(I:C)-treated mice, and mice treated with RVX208 were indistinguishable from those that received poly(I:C) treatment alone (Figure 3A).

***Lung fibrosis assessments.*** To assess the distribution and degree of fibrosis in whole lung, we used high-resolution microcomputed tomography (micro-CT) imaging *in vivo* to systematically analyze the effects of poly(I:C) on airway remodeling, comparing the morphological features of PBS-treated animals with those of the poly(I:C) and poly(I:C) + ZL0454 treatment groups. In this approach, multiplanar images were acquired over regular breathing patterns under controlled anesthesia. For comparison, the cross-sectional area at the level of the sixth thoracic vertebra was measured on the transverse views (Figure 3B). Consistent with our earlier observations, poly(I:C) induced a significant increase in parenchymal radiodensity caused by lung remodeling and increases in collagen content, most consistently in the left lower lobe (Figure 3B). In contrast, significantly fewer poly(I:C)-induced changes in tissue radiodensity were observed noninvasively in micro-CT images of ZL0454-treated mice (Figure 3B). Furthermore, the calculation of the cross-sectional area showed that the poly(I:C) treatment demonstrated a significant decrease in cross-sectional area, suggesting a component of restrictive airway disease (Figure 3D). However, this reduction was prevented in animals treated with ZL0454 (Figure 3D).

A systematic analysis of the micro-CT images of the mouse lungs demonstrates the influence of poly(I:C) treatment, which resulted in increasing the tissue radiodensity (Figures 3C and 3E), an effect that was prevented by treatment with ZL0454 (Figures 3C and 3E). Collectively, these data indicated that repetitive activation of the TLR3 pathway produced extensive remodeling primarily in the left lower lobe of the lung, as evidenced by micro-CT images used to assess the presence or absence of changes in tissue density in control versus treated animals.

Microscopy (using the method of multiphoton microscopy combined with second harmonic generation microscopy) (27) provided a three-dimensional representation of lung fibrosis (second harmonic generation microscopy;

Figure 3F, green) throughout the full lung structure (multiphoton microscopy; Figure 3F, red), avoiding the bias of sectioning (30). A marked pattern of peribronchial collagen deposition was observed tracking with the major bronchioles and smaller conductive airways (Figure 3F). These data indicate that TLR3-driven, innate inflammation–induced remodeling results in increased peribronchial and subepithelial collagen deposition.

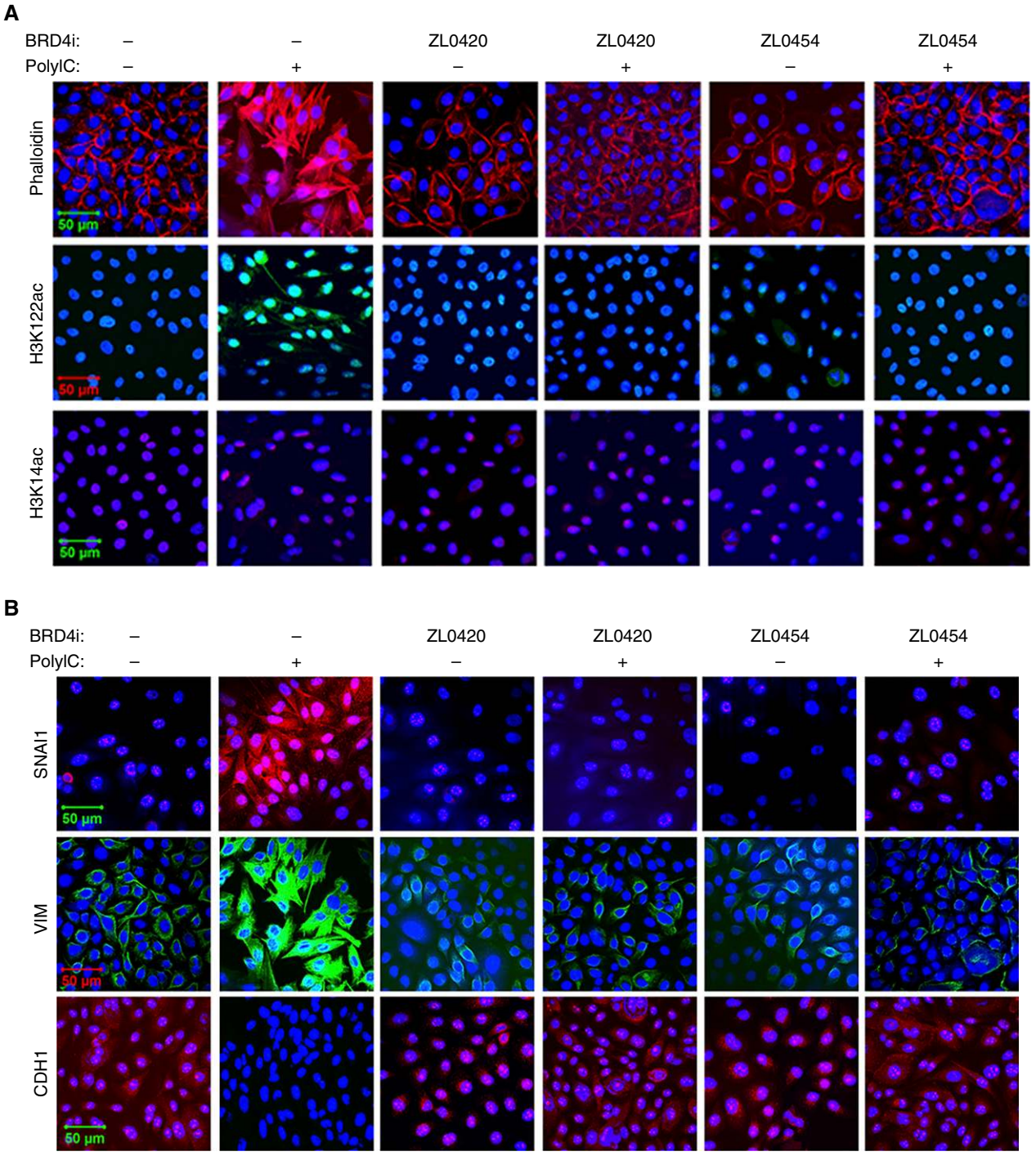


**Figure 2.** Effect of selective BRD4 inhibitors (BRD4i) on mesenchymal transition. hSAECs were untreated or stimulated with poly(I:C) for 12 days in the absence or presence of the indicated BRD4i. Shown are confocal immunofluorescence micrographs after staining with Alexa 568–conjugated phalloidin (red color), anti-H3K122Ac, and anti-H3K14Ac (*A*), or anti-SNAI1, anti-VIM, and anti-CDH1 antibodies (*B*) as indicated. Each slide was counterstained with DAPI (a nuclear DNA stain, blue color). (*C*) Quantification of fluorescence intensity (FI) in five independent fields, shown as the fold change over unstimulated cells (ImageJ). $^{*}P < 0.01$ compared with PBS; $^{\#}P < 0.01$ compared with poly(I:C)-treated cells. Scale bars: 50 μm.

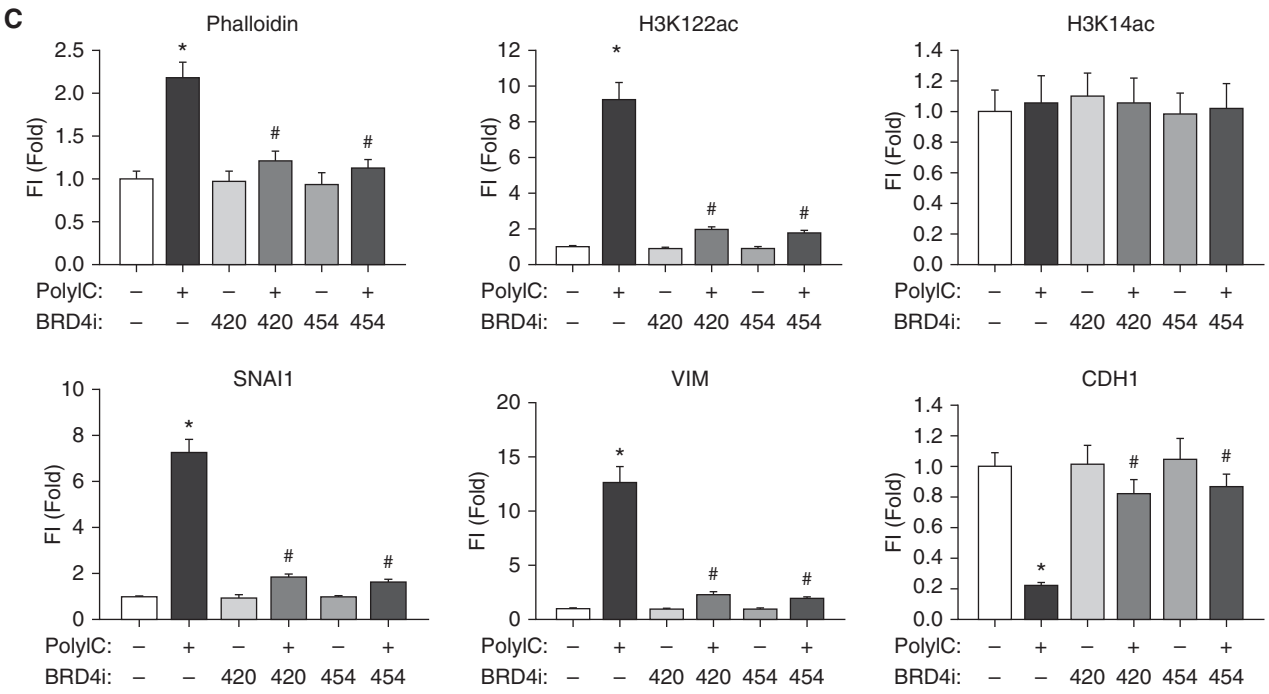


**Figure 2.** (Continued).

### Histological Analysis of the Effects of BRD4 Inhibitors on TLR3-induced Airway Remodeling

We evaluated the correlation between the changes observed by micro-CT and tissue fibrosis by comparing the changes in radiodensity with histological Masson's trichrome stains of lung sections. In untreated animals, poly(I:C) induced marked epithelial hypertrophy, disruption of the epithelial barrier with subepithelial myofibroblast expansion, interstitial collagen deposition, and alveolar hypercellularity/inflammation (Figure 4A). By contrast, these effects were largely mitigated by ZL0454 and ZL0420 treatments, which restored the epithelial morphology, reduced subepithelial collagen deposition, and reduced subepithelial myofibroblast expansion (Figure 4A). Although JQ1 showed minor improvements in fibroblast expansion and alveolar inflammation, RVX208 had no effect at the doses used (not shown).

The effect of the selective BRD4 inhibitors on global fibrosis and collagen content was quantified by modified Ashcroft scoring (31). In untreated animals, poly(I:C) increased the Ashcroft score to 9.5, which was reduced to 1 by the selective BRD4 inhibitors (Figure 4B); this effect was statistically significant ($P = 0.018$). JQ1 reduced the Ashcroft score to an intermediate level, 5.2 ($P = 0.037$ compared with poly(I:C) alone), whereas RVX208 reduced the effect to 8.4 (not significant compared with vehicle-treated animals). Similarly, a more than threefold increase in the hydroxyproline content of the BAL fluid was nearly normalized by the selective BRD4 inhibitors ZL0454 and ZL0420, with JQ1 showing an intermediate effect and RVX208 showing no effect (Figure 4C). A similar pattern of reduced collagen accumulation was observed in measurements of total lung hydroxyproline content (Figure 4D).

### Effects of BRD4 Inhibition on Airway Responsiveness and Lung Physiology

In allergic airway remodeling, increased peribronchial subepithelial collagen deposition can contribute to fixed airways obstruction, whereas airway smooth muscle hypertrophy/hyperplasia can contribute to enhanced bronchoconstrictive responses to allergens (9, 32). To determine the effects of innate inflammation–induced airway remodeling on airway physiology and its dependence on BRD4, we assessed control mice, poly(I:C)-treated mice, and poly(I:C)-treated mice treated with ZL0454 using a FlexiVent. As shown in Figures 5A–5C, dynamic measures of lung resistance (R), tissue damping (G), and elastance (stiffness [H]) in mice administered poly(I:C) were elevated, indicating hyperresponsiveness to methacholine (MCh), which is suggestive of enhanced bronchoconstrictive responses and changes in lung tissue secondary to the development of fibrosis. ZL0454 treatment resulted in significant reductions in these measures, and the reestablishment of lung resistance, tissue damping, and elastance profiles to levels similar to those observed in control (PBS-treated) mice. In similarity to the dynamic measurements, passively measured constitutive lung tissue characteristics (no MCh) in mice administered poly(I:C) demonstrated significant changes in lung tissue impedance (Figure 5D) and decrements in lung compliance (Figures 5E and 5F), consistent with the development of enhanced tissue stiffness. These effects were reversed with ZL0454 treatment. Further analysis of the dynamic relationships demonstrated significant changes in lung hysteresivity (G/H) (Figure 5G), which was reversed with ZL9454 treatment. Analyses of the expiratory compliance curves from mice administered poly(I:C) demonstrated decrements in the Salazar-Knowles parameter (indicating a decreased lung compliance curve slope) (Figure 5H), and a decreased cumulative

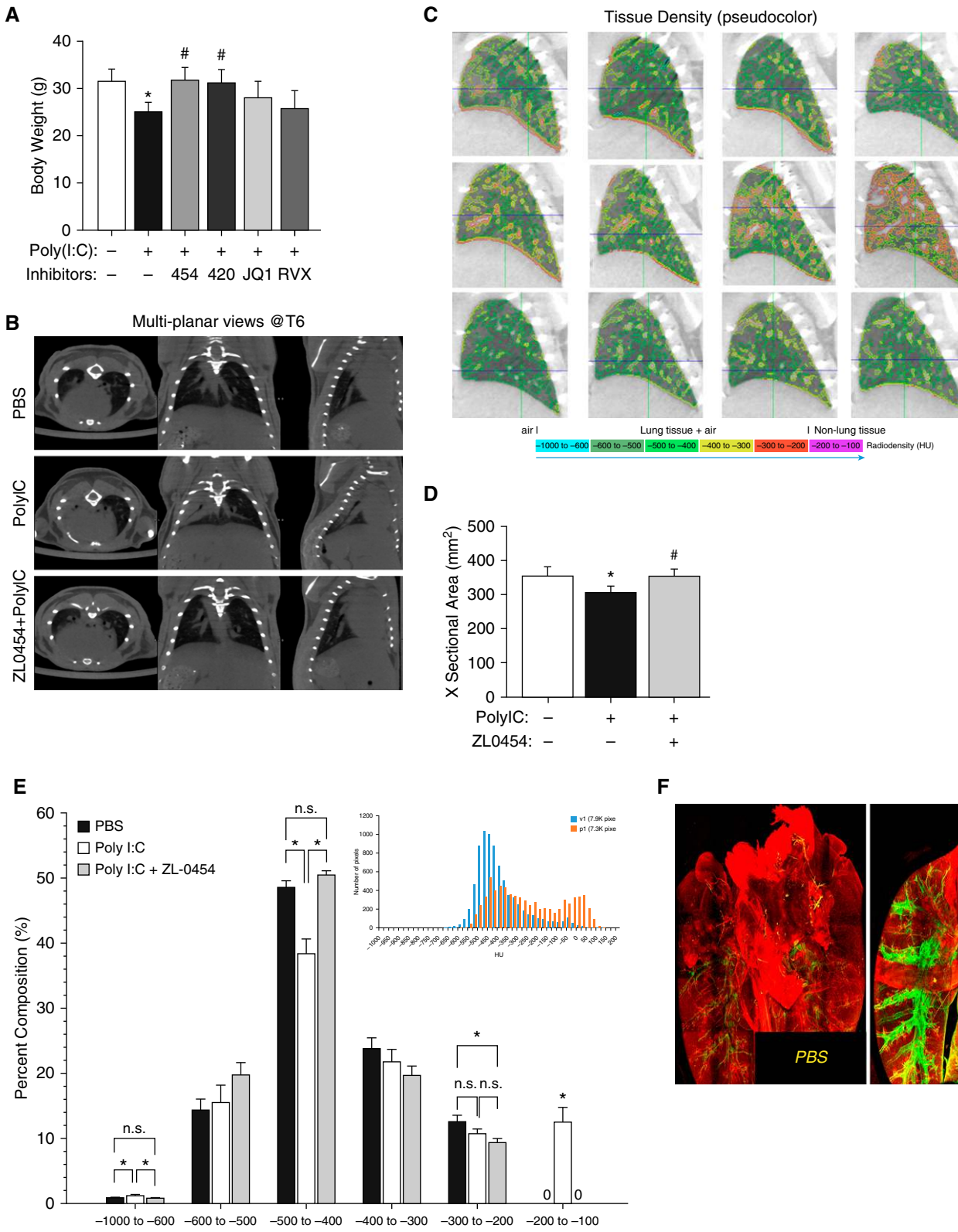


**Figure 3.** Effects of BRD4 inhibitors on repetitive poly(I:C)-induced fibrosis. (*A*) Effect of treatments on group body weight. Shown is the mean body weight for each treatment group ($n$ = 6 mice). $^{*}P < 0.01$ compared with PBS-treated controls; $^{\#}P < 0.01$ compared with poly(I:C)-treated mice. (*B*) Multiplanar views at thoracic vertebrae T6. Shown in PBS, poly(I:C), and ZL0454 + poly(I:C) groups; $n$ = 9. (*C*) Pseudocolor representations of lung density. Single virtual slices of lung micro–computed tomography (CT) images of four individual mice per group, treated with PBS (control), poly(I:C), or poly(I:C) + ZL0454

area under the expiratory compliance curve (Figure 5I). Overall, similar to what was found with the dynamic measurements (Figures 5A–C and 5G), treatment with ZL0454 reversed the changes observed in passively measured constitutive lung tissue properties induced by poly(I:C) (Figures 5D–5F, 5H, and 5I).

### BRD4 Inhibitors Block Inflammation-induced Mesenchymal Transition *In Vivo*

Repetitive TLR3 inflammation results in mesenchymal transition in nonciliated epithelium lining the small bronchioles of the airway, characterized by *de novo* expression of the mesenchymal transcription factors and ECM-modifying proteins (27). To examine the effect of BRD4 inhibitors on this inducible mesenchymal transition, we assessed mesenchymal transition using gene expression and immunofluorescence microscopy. First, total lung mRNA was extracted and the expression of mesenchymal transition programs was measured by qRT-PCR. In a manner consistent with our earlier studies, repetitive poly(I:C) stimulation resulted in a 3.1-fold increase in murine (m) *SNAI1* expression; this induction was completely inhibited in the animals treated with ZL0454 and ZL0420 (Figure 6A). When we quantified the expression of mesenchymal intermediate contractile proteins, we observed that poly(I:C) produced a 6.9-fold increase in *mVIM*, an effect that was also completely reversed by ZL0454 and ZL0420. Analysis of the mesenchymal core transcription factors showed that poly(I:C) produced a 7.8-fold increase in *mα-SMA*, a 7.3-fold increase in *mCOL1A*, a 9.7-fold increase in *mFN1*, and a 6.3-fold increase in *mMMP9* mRNAs. These inductions were all significantly reduced by the BRD4 inhibitors (Figure 6A). In addition to inhibition of the 5.9-fold upregulated *mIL6* mRNA, a 4.3-fold increase of the NF-κB–dependent *mKC* gene was similarly reduced by both BRD4 inhibitors. Meanwhile, both ZL0420 and ZL0454 also induced mHEXIM1 expression, indicating that these compounds interacted with BRD4 in the mouse lung tissue (Figure E3) (23).

To confirm the functional inhibition of BRD4 HAT activity at the protein level, we conducted immunofluorescence microscopy on the unique H3K122Ac product. Poly(I:C) induced a striking 12.6-fold increase in mucosal H3K122Ac staining, and this effect was reduced to control levels by either ZL0420 or ZL0454 treatment (Figure 6B). This result indicated that the target of the BRD4 inhibitors was activated and directly reduced by BRD4 inhibitor treatment *in vivo*. Correspondingly, the 14.3-fold upregulation of SNAI1, the 11.2-fold increase of FN1, and the 17.6-fold increase of mucosal VIM produced by repetitive TLR3 activation was blocked by either BRD4 inhibitor (Figure 6B). All of these data indicated that the mucosal mesenchymal transition and BRD4 HAT activity induced by TLR3 signaling was inhibited by both ZL compounds.

Activated RelA binds to BRD4 (21, 22), an interaction that is mediated by the BRD4 BD domain, which is a target of BRD4 inhibitors (23). To measure this molecular interaction in the airway mucosa, we used a proximity ligation assay, which detects atomic-distance interactions between two molecules (22). After heterotypic antibody staining, oligonucleotide ligation, and PCR amplification, RelA–BRD4 interactions appear as fluorescent foci *in situ* (22). We observed that poly(I:C)-increased RelA–BRD4 binding was increased by 19.6-fold, and this interaction was disrupted by both ZL420 and ZL0454 treatment (Figure 6C).

### BRD4 Inhibitors Block Inflammation-induced Myofibroblast Transdifferentiation *In Vivo*

Myofibroblasts are a dynamic population of mesenchymal cells that play a fundamental effector role in ECM deposition in airway remodeling (9, 32, 33). To determine the effect of poly(I:C) on the myofibroblast population and understand the effect of BRD4 inhibitors on these profibrotic cells, we examined the presence of $\alpha$-SMA$^+$/COL1A$^+$ cells in the submucosa by immunofluorescence microscopy. Poly(I:C) induced a dramatic upregulation of both α-SMA and COL1A in the subepithelium (Figure E4A). The merged images indicate a robust increase in the $\alpha$-SMA$^+$/COL1A$^+$ myofibroblast population. An average of 36 costaining cells per high-power field were observed in the poly(I:C)-treated animals, compared with zero in the PBS-treated mice (Figure E4B, $P < 0.01$). Importantly, this population of cells was absent in the lungs from BRD4 inhibitor–treated mice (Figure E4B), indicating that TLR3 inflammation induces recruitment or transdifferentiation of the myofibroblast population.

### Poly(I:C)-induced Mesenchymal-transitioned Cells Produce BRD4-Sensitive Paracrine Factors that Induce Myofibroblast Transdifferentiation *In Vitro*

Subepithelial fibroblasts within the attenuated fibroblast sheath (collectively referred to as the epithelial–mesenchymal trophic unit) (34) play a key role in tissue differentiation, epithelial polarization, and airway remodeling in disease (35, 36). Previous studies have suggested that epithelial injury controls growth factors

**Figure 3.** (Continued). ($n$ = 9/group), showing tissue areas of low density (−1,000 to −600 HU) as green color, and areas of higher tissue density (−300 to −200 HU) as red color. Relative density ranges are as shown on the density color bar. Note the appearance of increased red coloration in mouse lungs with poly(I:C) administration, which reverts back toward green colorations, similar to control lungs, with ZL0454 treatment. (*D*) Quantitation of cross-sectional area at T6 ($n$ = 9 mice/group). (*E*) Comparison of whole-lung micro-CT tissue density. Density data from mice treated with PBS (control; black bars, $n$ = 9), poly(I:C) (white bars; $n$ = 9), and poly(I:C) + ZL0454 (gray bars; $n$ = 9), based on image analyses of lungs from each group, including those shown in *C*. Bars are means ± SE; *$P < 0.05$; n.s. = not significant for comparisons indicated by brackets; 0 = density signal not detected for PBS and poly(I:C) + ZL0454 groups, at the highest density range of −200 to −100 HU. Inset: micro-CT image signal histograms of an example comparison of the volume of lung tissue over the full range of tissue density for a single whole lung from a control (PBS-treated) mouse (blue bars), and a mouse administered poly(I:C) (red bars), showing a significant rightward shift in the density signal consistent with lung tissue of higher density, which is associated with development of lung fibrosis. (*F*) Visualization of collagen accumulation via second harmonic generation microscopy (SHGM). Two-photon cross-sections show collagen deposition around the airways in the PBS and poly(I:C) groups. Contrast is provided by tissue autofluorescence (red) and SHGM collagen signal (green). This is a mosaic image; for details see Supplementary Methods and Materials in the data supplement. HU = Houndsfield units.

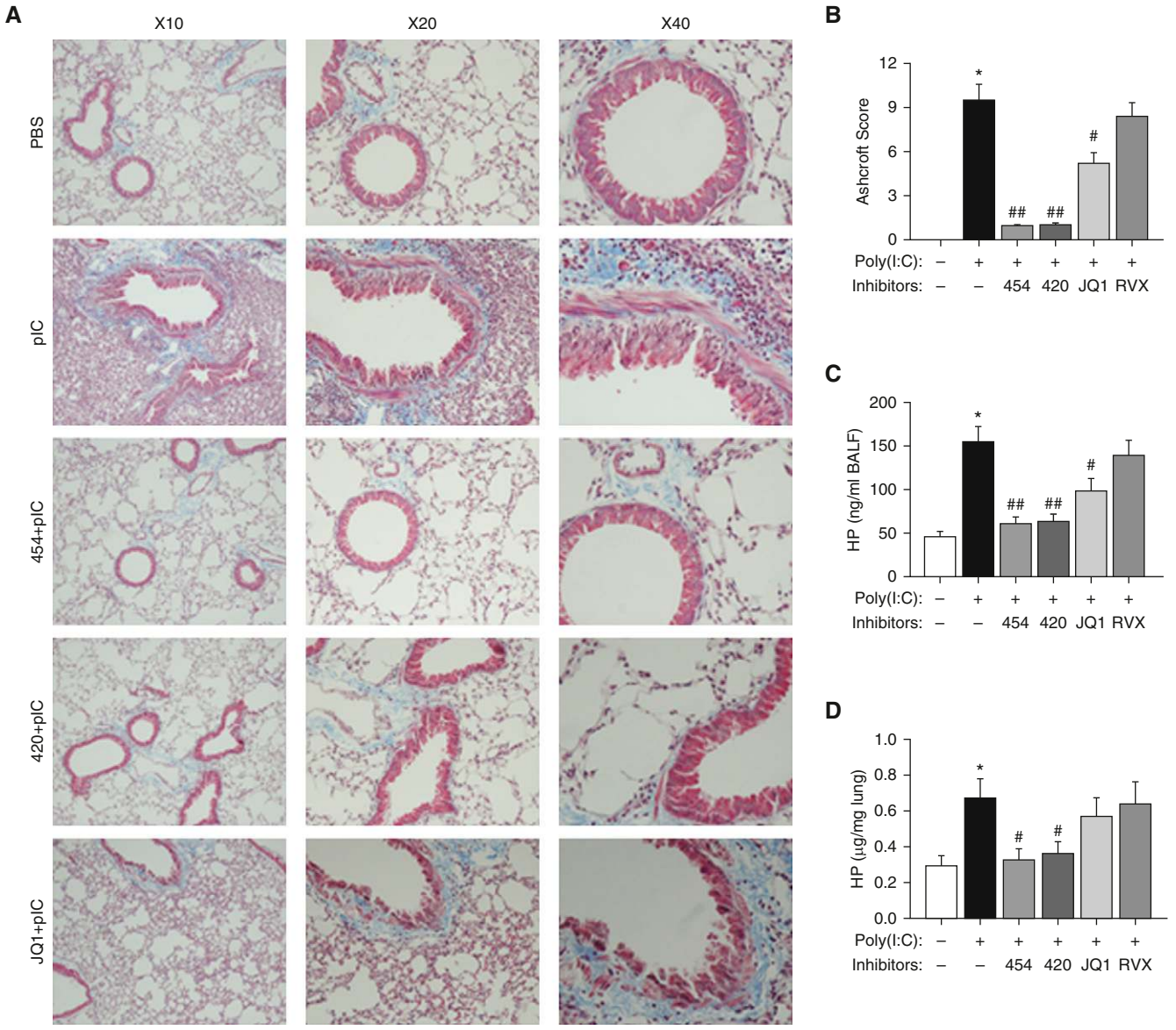


**Figure 4.** Histological assessment of airway remodeling and fibrosis. (*A*) Masson's trichrome staining of a representative lung section at 10×, 20×, and 40× magnification as indicated. Note the epithelial barrier disruption, myofibroblast expansion, and collagen (blue) deposition in the subepithelial and interstitial spaces in the poly(I:C)-treated group, which are largely reversed by the ZL0454 and ZL0420 treatments. (*B*) Modified Ashcroft scoring for treatment groups; $n = 6$ in each group. (*C*) Hydroxyproline (HP) content of BAL fluid (BALF). Shown is the mean hydroxyproline measurement for BALF from $n = 6$ mice in each treatment group. $^{*}P < 0.01$ compared with PBS-treated controls; $^{\#}P < 0.05$ compared with poly(I:C)-treated mice; $^{\#\#}P < 0.01$ compared with poly(I:C)-treated mice. (*D*) Hydroxyproline content of lung tissue; $n = 6$ in each group. pIC = poly(I:C).

that control myofibroblast proliferation (37). To determine whether the TLR3 signaling–induced mesenchymal state affects epithelial–fibroblast interactions, and whether such interactions require BRD4 signaling, we adapted a coculture system. HSAECs were cultured under basal conditions or transitioned into the mesenchymal state by chronic poly(I:C) stimulation in the absence or presence of the ZL0454 inhibitor and seeded on Millicell filters. After 48 hours, the inserts were extensively washed free of the inducer/inhibitor and transferred into a submerged culture of normal human lung fibroblasts (NHLFs) (Figure 7A). At this point, the hSAECs were in mesenchymal transition, as demonstrated by the presence of actin stress fibers and enhanced VIM expression (Figure 7B). Next, we examined the phenotype of the underlying NHLFs. The hSAECs that were induced into mesenchymal transition by poly(I:C) triggered a myofibroblast transdifferentiation characterized by enhanced α-SMA and phalloidin staining in immunofluorescence microscopy. Also, the EMT hSAEC-mediated myofibroblast transdifferentiation of NHLFs was completely blocked by ZL0454 treatment (Figure 7C). A similar pattern was observed in the 3.8-fold upregulation of *α-SMA*, the threefold upregulation of *COL1A*, and the 2.8-fold upregulation of *FN1* mRNAs (Figure 7D). All of these increases were reduced to the levels observed for NHLFs in the hSAECs treated with poly(I:C)

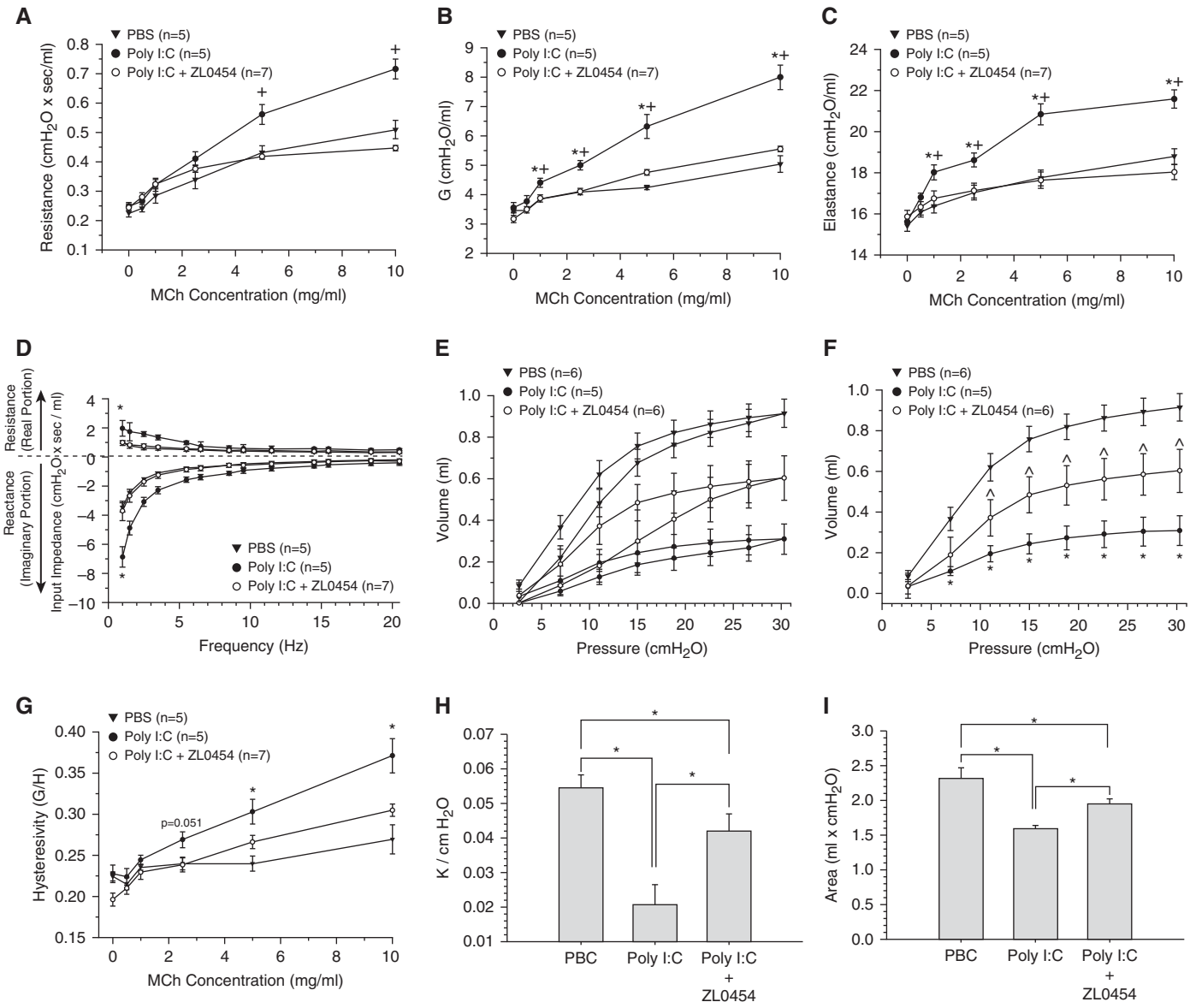


**Figure 5.** Effect of BRD4 inhibitors on poly(I:C)-induced changes in dynamic and constitutive lung characteristics. Lung-function variables measured in mice treated with PBS (control; solid inverted triangle), poly(I:C) (solid circle), and poly(I:C) + ZL0454 (open circle), with mouse group numbers as shown in the respective graph keys or as below: (*A*) resistance; (*B*) tissue damping (G); (*C*) elastance (stiffness); (*D*) impedance; (*E*) full lung compliance curves; (*F*) expiratory lung compliance curves. $^{\wedge} = P < 0.05$ compared to poly(I:C) alone; (*G*) hysteresivity (G/H); (*H*) Salazar-Knowles (slope) parameter (K) of expiratory lung compliance curves in *F*, $^{*}P < 0.05$ as indicated by brackets, respective mouse group $n = 5$, 7, and 7; (*I*) area under expiratory lung compliance curves in *F*, $^{*}P < 0.05$ as indicated by brackets, respective mouse group $n = 5$, 7, and 5. For all line-graph figures, $^{*}P < 0.05$ versus PBS, $^{+}P < 0.05$ versus poly(I:C) + ZL0454. MCh = methacholine.

and ZL0454. We conclude that TLR3-mediated inflammation induces a BRD4-dependent paracrine release of soluble factors that control myofibroblast transdifferentiation.

## Discussion

Viral upper-respiratory-tract infections are repetitive and chronic, and are responsible for periodic exacerbations of asthma and chronic obstructive pulmonary disease. These exacerbations necessitate unscheduled medical visits and are linked to a progressive decline in pulmonary function (6, 7, 38). Mechanistically, viral injury produces cellular adaptive changes that result in epigenetic reprogramming and structural remodeling of the airway through poorly understood mechanisms. The results we obtained from this model of repetitive innate inflammation indicate that the airway epithelium is highly adaptive to innate stimulation. It can reprogram its genome to enable mesenchymal transition and the expression of ECM-remodeling proteins and paracrine factors that expand the myofibroblast population within the epithelial–mesenchymal trophic unit. Dysregulation of epigenetic modifying enzymes was recently demonstrated in

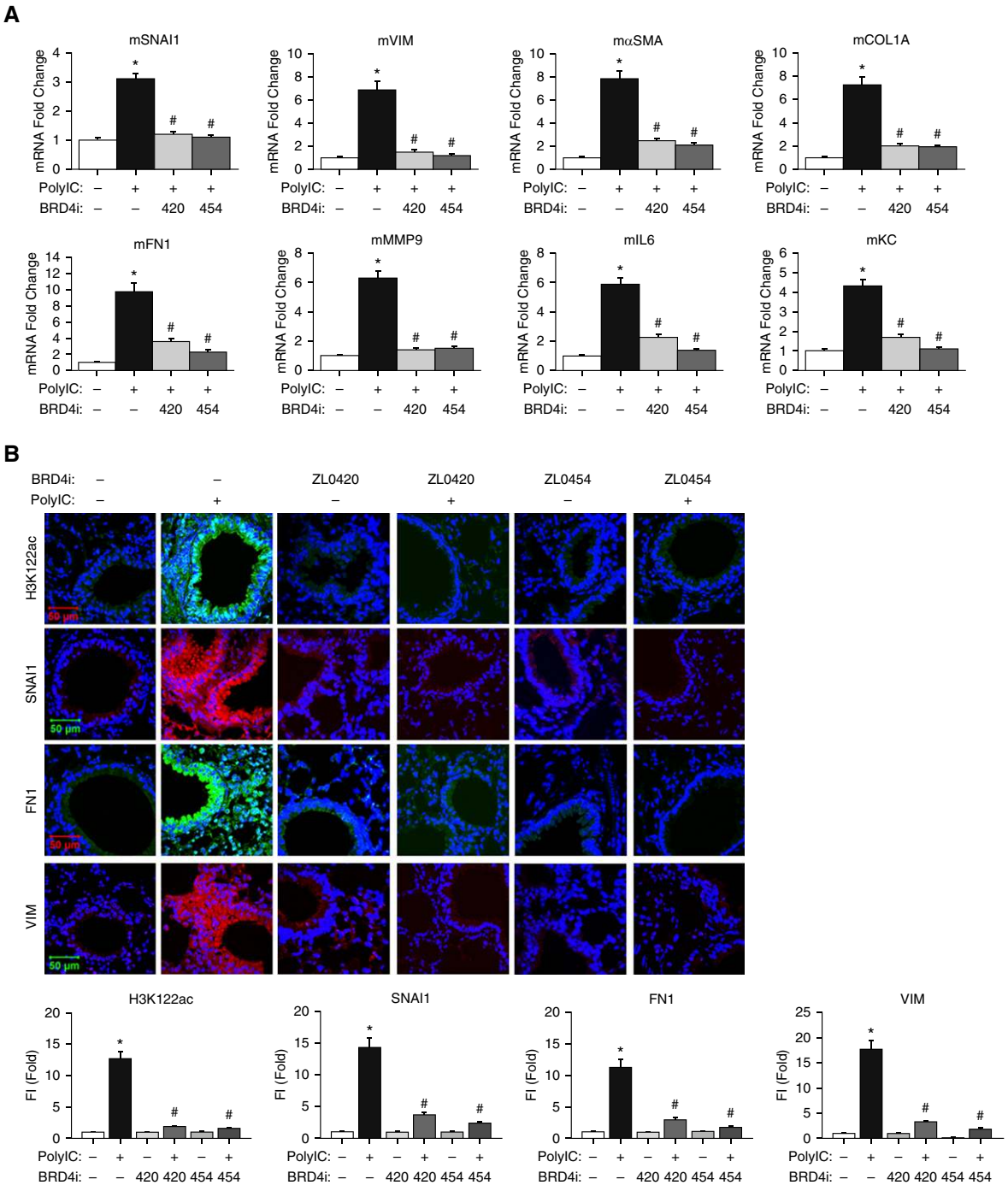


**Figure 6.** BRD4 inhibitors block the TLR3 agonist–induced epithelial–mesenchymal transition (EMT) program *in vivo*. (*A*) Analysis of the effect of BRD4i on induction of the fibrotic and EMT program. Total lung RNA was extracted, purified, and reverse transcribed. The abundance of the indicated mRNAs was determined using mouse gene–selective primers. Shown is the mean fold-change mRNA abundance (± SD) normalized to mouse cyclophilin (*mPPIA*) for $n = 5$ animals from each treatment group. $^{*}P < 0.01$ compared with PBS-treated controls; $^{\#}P < 0.01$ compared with poly(I:C)-treated mice; $n = 6$ in each group. (*B*) Induction of the mesenchymal program in the airway. For each treatment group, lung sections were fixed, permeabilized, and incubated with anti-H3K122Ac, SNAI1, FN1, and VIM antibodies, and then stained with Alexa Fluor 488– or Alexa Fluor 568–conjugated goat anti-rabbit IgGs (shown in green or red, respectively), counterstained with DAPI, and imaged via confocal fluorescence microscopy. On the right is the mean FI determined in five sections. $^{*}P < 0.01$ compared with PBS-treated controls; $^{\#}P < 0.01$ compared with poly(I:C)-treated mice; $n = 6$ in each group. (*C*) *In situ* proximal ligation assay (PLA) of RelA·BRD4 complex formation. Paraffin-fixed tissue sections from PBS-, poly(I:C)-, or poly(I:C) + BRD4i–treated mice were subjected to PLA using anti-mouse BRD4 and anti-rabbit RelA antibodies. Nuclei are counterstained in DAPI (blue); interacting proteins appear as red foci. Images were acquired by confocal microscopy at ×63 magnification. Note the intense foci formed in the epithelium. Right: quantification of FI. $^{*}P < 0.01$ compared with PBS-treated controls; $^{\#}P < 0.01$ compared with poly(I:C)-treated mice; $n = 6$ in each group. Scale bars: 50 μm.

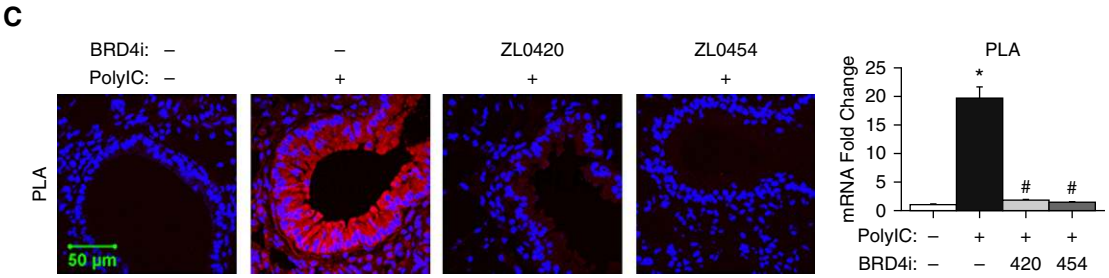


**Figure 6.** (Continued).

airway epithelial cells and fibroblasts derived from patients with asthma (39). Our study extends that observation to demonstrate that epigenetic reprogramming is functionally mediated by BRD4 HAT in inflammation-induced mesenchymal transition *in vitro* and airway remodeling *in vivo*. A surprising finding from our earlier studies was that chronic TLR3-mediated activation triggers mesenchymal transition through an IκB kinase–NF-κB pathway (27). In the present study, we advance this understanding to demonstrate that chronic TLR3 ligation triggers NF-κB/RelA·BRD4 complex formation, a step linked to BRD4 HAT activation, followed by NF-κB–dependent targeting BRD4 HAT to innate and mesenchymal gene expression programs (21, 22). Although previous work has shown that BRD4 is required for mesenchymal transition mediated by the TGF-β growth factor (21, 40), the role of BRD4 in innate inflammation-induced mesenchymal transition has not been demonstrated. Our studies show that BRD4 HAT is required for poly(I:C) to induce CDH1 downregulation, activate expression of core mesenchymal transactivators, stimulate ECM remodeling, and secrete paracrine factors for myofibroblast transition, playing a central role in inflammation remodeling.

### Chemical Probes Reveal that BRD4 Plays a Central Role in Inflammation Remodeling

Our mechanistic studies have shown that BRD4 is a central mediator of the growth factor–induced mesenchymal transition triggered by NF-κB/RelA activation (21). BRD4 is a member of a superfamily of BET family proteins, sharing the BD motif. Within the BET family, BRD4 is unique in that it interacts with the CDK9-containing transcriptional elongation complex through its C-terminal tail. Previously, we have shown how activated NF-κB complexes with BRD4 and controls antiviral innate immunity (20, 22), as well as the initiation of so-called "type II" EMT (mesenchymal transition of normal cells) (18), by activating gene expression programs involving transcriptional elongation. The findings of enhanced H3K122Ac formation by poly(I:C) exposure and its inhibition by BRD4 inhibitors provide direct evidence that BRD4 HAT activity is inducible by the innate signaling pathway *in vivo*. H3K122Ac is a histone modification that enables histone repositioning to promote transcriptional elongation of the NF-κB–regulated mesenchymal program (25). Our current findings *in vitro* and *in vivo* validate BRD4 HAT as a potentially viable therapeutic target for the modulation of airway remodeling in response to viral inflammation.

The development of small-molecule inhibitors of BRD4 has been the subject of intense efforts because of its role in malignancy and metastatic disease (28, 41). Currently, no commercially available small-molecule inhibitor is highly BRD4 selective (41). Our recent development and validation of ZL0454 as a highly specific BRD4 inhibitor with nanomolar binding affinity and 30-fold specificity over the closely related BRD2 isoform will advance the field by providing a useful probe for testing the role of BRD4 in pathophysiological conditions *in vivo* (23).

The mechanism by which BD-targeted inhibitors disrupt BRD4-dependent transcription is believed to involve multiple actions. These include our finding that RelA recruitment and Pol II phosphorylation are disrupted by BD-directed small-molecule inhibitors, indicating that the BRD4 BD plays a central role in coordinating the formation of a stable preinitiation complex (23, 24). Similarly, BRD4 BD inhibitors displace BRD4 from high-affinity chromatin-binding sites (23, 42) and disrupt the multiple protein–protein interactions that are necessary for BRD4 function, including those with Pol II and RelA (23, 43). Because of these complex actions, BRD4 is an attractive therapeutic target for the modulation of airway remodeling in viral infection–induced remodeling. Importantly, in the present study, our highly selective small-molecule BRD4 inhibitors showed no evidence of systemic toxicity at doses that interfered with BRD4 action *in vivo*. Thus, we believe that their application will advance our understanding of the role of BRD4 in the cell-state transitions that underlie airway remodeling.

### Viral Pattern–induced Remodeling Produces Functional Changes in Airway Physiology

The poly(I:C)-associated increases in both dynamic lung tissue damping (which indicates increased tissue resistance to lung expansion; Figure 5B) and dynamic lung stiffness (as elastance [H]; Figure 5C) are consistent with changes in lung tissue characteristics that would be expected to be associated with the development of lung fibrosis. Similarly, the increases in dynamic lung resistance with MCh (Figure 5A) and the increased constitutive resistance portion of the impedance parameter (as the real portion; Figure 5D) are likewise indicative of increased airway and lung tissue resistances to airflow resulting from poly(I:C) administration and the development of fibrosis. Furthermore, the significant decrease in lung compliance, the compliance slope parameter, and the area under the compliance curve (Figures 5E, 5F, 5H, and 5I) observed with poly(I:C) administration are also consistent with changes in lung characteristics that would be associated

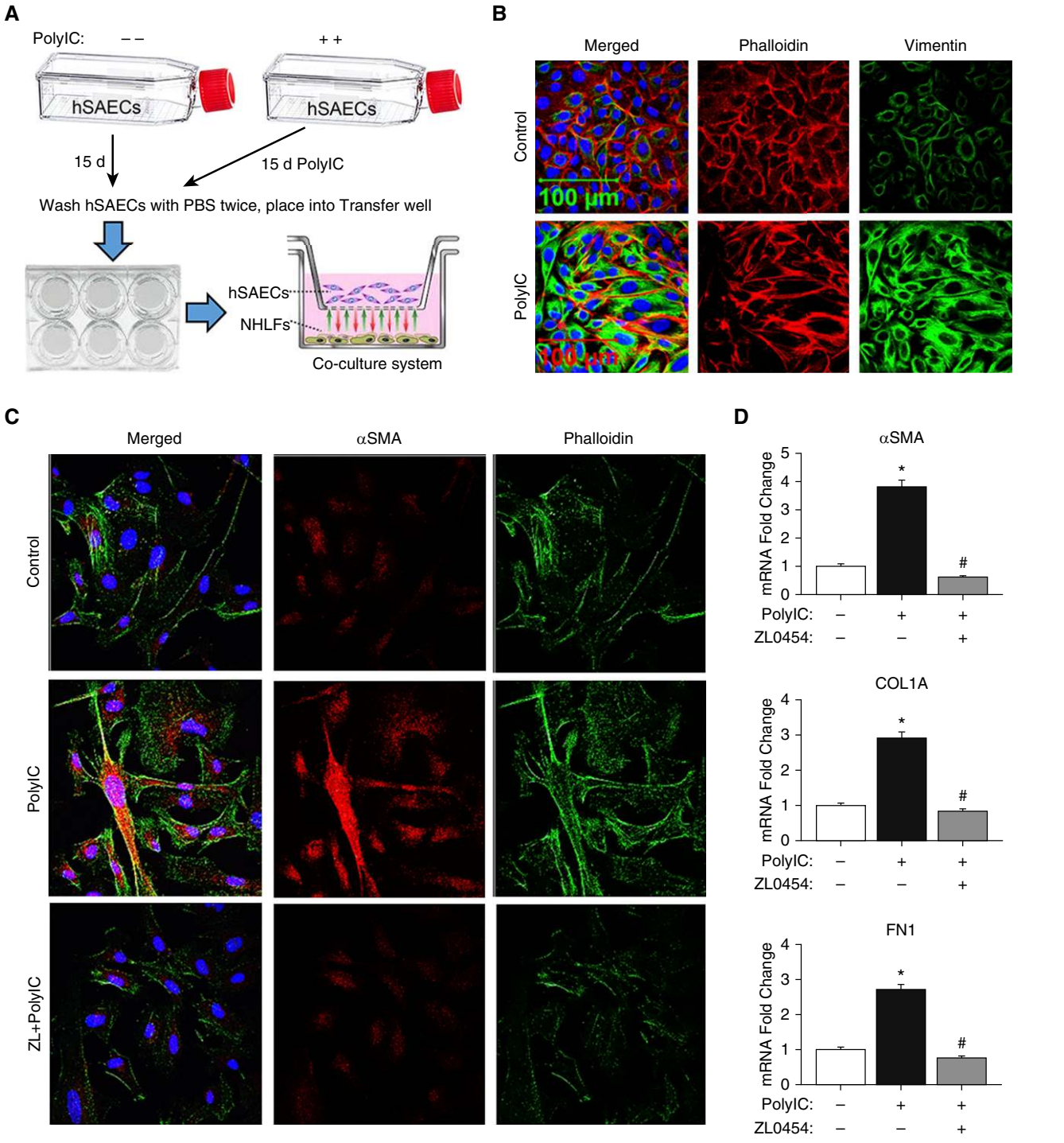


**Figure 7.** Poly(I:C)-induced EMT triggers the secretion of paracrine factors that promote myofibroblast transdifferentiation. (*A*) Experimental strategy. hSAECs were stimulated in the absence or presence of poly(I:C) ± ZL0454 for 15 days to induce mesenchymal transition. Afterward, the cells were washed free of inducer and assembled in Millicell inserts over normal human lung fibroblasts (NHLFs) in submerged culture. (*B*) Mesenchymal state of overlying hSAECs. hSAECs were stained with phalloidin (red) or VIM (green) to confirm the presence of poly(I:C)-induced mesenchymal transition. Scale bars: 100 μm. (*C*) Myofibroblast state of NHLFs. Confocal immunofluorescence images of NHLFs stained with anti–α-SMA (red) or phalloidin (green). Images taken at the same magnification as in *B*. Note the induction of $\alpha$-SMA$^{+}$/phalloidin$^{+}$ cells in the merged image by the hSAECs in the EMT state. (*D*) Induction of the myofibroblast gene-expression program. Total RNA from NHLFs were extracted and subjected to qRT-PCR for *α-SMA*, *COL1A*, and *FN1* mRNA. $^{*}P < 0.01$ compared with NHLFs cocultured with normal hSAECs; $^{\#}P < 0.01$ compared with hSAECs induced by poly(I:C).

with the development of lung fibrosis. Importantly, each change in these dynamic and constitutive properties of the lung induced by poly(I:C) was inhibited with ZL0454 treatment, indicating an important role for BRD4 inhibition in the prevention of lung fibrosis and its attendant diminution of lung function.

### *In Vivo* Lung Imaging Analyses Indicate Inhibition of Lung Fibrosis with BRD4 Inhibition

Our histopathological findings, along with those from *in vitro* whole-lung microscopic imaging studies demonstrating poly(I:C)-induced changes in the collagen content of the lungs and the effectiveness of ZL0454 in inhibiting lung fibrosis, are consistent with the results of micro-CT imaging. Specifically, this analysis indicates that local changes in the radiodensity of lung tissue are caused by increases in collagen deposition. These observations are consistent with previous findings in the bleomycin model (44, 45), where a correlation between changes in mouse lung radiodensity and fibrosis characterized by excessive collagen deposition was validated by histopathological analysis. Micro-CT has several important advantages that enable researchers to perform longitudinal assessments of airway remodeling and identify heterogeneous patterns of fibrosis, which are characteristic of both the bleomycin model and innate inflammation–mediated remodeling. This validation approach will enable the application of micro-CT in future studies for longitudinal assessments of the heterogeneous patterns of fibrosis in inflammation-mediated remodeling.

Furthermore, the observations that we have made based on *in vitro* and *in vivo* whole-lung imaging studies are consistent with the poly(I:C)-dependent lung-function changes outlined above, such as an increase in lung stiffness (Figure 5C) and a decrease in both lung compliance (Figure 5F) and the Salazar-Knowles slope parameter (Figure 5H). The changes in whole-lung intermediate density and very high tissue density after poly(I:C) administration were likewise consistent with the significant increment in the G/H parameter (Figure 5G), which is considered to indicate a loss of functional lung volume and an increase in lung heterogeneity. Again, these changes in measured lung physical and responsiveness characteristics are consistent with fibrotic lung tissue modifications, which were particularly evident as the significant increase in the very-high-density tissue range (Figure 3E). As with the lung-function characteristics mentioned above, these poly(I:C)-dependent tissue-density modifications were inhibited by ZL0454 treatment, indicating that BRD4 inhibition may be a potent approach for inhibiting the development of lung fibrosis.

### Inflammation-induced Mesenchymal Transition Mediates Myofibroblast Expansion via a Paracrine Mechanism

The processes that control airway remodeling involve complex intercellular communication between the epithelium and stromal fibroblasts. Asthma exacerbations associated with disruption of the epithelial barrier induce the secretion of epithelial growth factors (TGF-β and epidermal growth factor) and cytokines (e.g., periostin, IL-17, and IL-11) that are important for mucosal repair (46). Our studies link the presence of stable EMT in the airways produced by innate inflammation with expansion of the subepithelial myofibroblast population. Myofibroblasts are central effector cells that are responsible for excessive ECM deposition of COL-I, COL-III, and FN1 in the lamina reticularis. The myofibroblast population is dynamic, increasing during the late phase of allergic inflammation (36), refractory asthma (47), and actively progressing chronic obstructive pulmonary disease or recurrent asthma (48). Pulmonary myofibroblasts originate from a variety of sources, including resident mesenchymal cells, epithelial and endothelial cells undergoing mesenchymal transition (EMT/EndoMT), perivascular fibroblasts (pericytes), and circulating bone marrow stem cells ("fibrocytes") (8, 49, 50). Our study was not designed to differentiate between these populations, but rather to determine whether stromal fibroblasts respond to paracrine factors secreted from mesenchymal-transitioned cells and then transition to functionally active myofibroblasts. Our demonstration that ZL0454 blocks the expression of these paracrine factors provides a mechanistic insight into how BRD4 inhibitors interfere with innate inflammation–driven fibrosis.

Our work has implications for the mechanisms and consequences of frequent viral-induced exacerbations in humans with chronic airway disease, informing a potentially viable strategy to prevent structural airway remodeling under those conditions. Importantly, our validation of the activation of the NF-κB–BRD4 pathway and its therapeutic effect in blocking airway remodeling and sensitization may be used in future therapeutic approaches to modify pathological responses to airborne pathogen exposures. Our current work also indicates that BRD4 inhibition can inhibit airway inflammation, remodeling, and myofibroblast expansion associated with cat dander exposure, suggesting that the BRD4 pathway is an important mediator in coupling innate and adaptive immune responses. These data identify BRD4 as an attractive target for developing novel epigenetic treatments for allergen- and virus-associated airway inflammation, and possibly control of airway remodeling. ■

**Author disclosures** are available with the text of this article at www.atsjournals.org.

**Acknowledgment:** The authors thank the University of Texas Medical Branch Histopathology Core, Inhalation Toxicology Core, and Optical Imaging Core, within The Center for Biomedical Engineering, for core laboratory support.

## References

1. Akinbami LJ, Moorman JE, Bailey C, Zahran HS, King M, Johnson CA, *et al*. Trends in asthma prevalence, health care use, and mortality in the United States, 2001-2010. *NCHS Data Brief* 2012;(94):1–8.
2. Busse WW, Lemanske RF Jr. Asthma. *N Engl J Med* 2001;344: 350–362.
3. Busse WW, Lemanske RF Jr, Gern JE. Role of viral respiratory infections in asthma and asthma exacerbations. *Lancet* 2010;376:826–834.
4. Lange P, Parner J, Vestbo J, Schnohr P, Jensen G. A 15-year follow-up study of ventilatory function in adults with asthma. *N Engl J Med* 1998; 339:1194–1200.
5. Peat JK, Woolcock AJ, Cullen K. Rate of decline of lung function in subjects with asthma. *Eur J Respir Dis* 1987;70:171–179.

6. Calhoun WJ, Haselkorn T, Miller DP, Omachi TA.Asthma exacerbations and lung function in patients with severe or difficult-to-treat asthma. *J Allergy Clin Immunol* 2015;136:1125–1127.e4.
7. O'Byrne PM, Pedersen S, Lamm CJ, Tan WC, Busse WW; START Investigators Group. Severe exacerbations and decline in lung function in asthma. *Am J Respir Crit Care Med* 2009;179: 19–24.
8. Noble PW, Barkauskas CE, Jiang D. Pulmonary fibrosis: patterns and perpetrators. *J Clin Invest* 2012;122:2756–2762.
9. Al-Muhsen S, Johnson JR, Hamid Q.Remodeling in asthma. *J Allergy Clin Immunol* 2011;128:451–462; quiz 463–454.
10. Bousquet J, Jeffery PK, Busse WW, Johnson M, Vignola AM. Asthma. From bronchoconstriction to airways inflammation and remodeling. *Am J Respir Crit Care Med* 2000;161:1720–1745.
11. Dransfield MT, Kunisaki KM, Strand MJ, Anzueto A, Bhatt SP, Bowler RP, *et al*.; COPDGene Investigators. Acute exacerbations and lung function loss in smokers with and without chronic obstructive pulmonary disease. *Am J Respir Crit Care Med* 2017;195: 324–330.
12. Royce SG, Cheng V, Samuel CS, Tang MLK. The regulation of fibrosis in airway remodeling in asthma. *Mol Cell Endocrinol* 2012;351: 167–175.
13. Prakash YS, Halayko AJ, Gosens R, Panettieri RA Jr, Camoretti-Mercado B, Penn RB; ATS Assembly on Respiratory Structure and Function. An Official American Thoracic Society research statement: current challenges facing research and therapeutic advances in airway remodeling. *Am J Respir Crit Care Med* 2017; 195:e4–e19.
14. Fedorov IA, Wilson SJ, Davies DE, Holgate ST. Epithelial stress and structural remodelling in childhood asthma. *Thorax* 2005;60: 389–394.
15. Davies DE. The role of the epithelium in airway remodeling in asthma. *Proc Am Thorac Soc* 2009;6:678–682.
16. Lambrecht BN, Hammad H. The airway epithelium in asthma. *Nat Med* 2012;18:684–692.
17. Kalita M, Tian B, Gao B, Choudhary S, Wood TG, Carmical JR, *et al*. Systems approaches to modeling chronic mucosal inflammation. *Biomed Res Int* 2013;2013:505864.
18. Tian B, Li X, Kalita M, Widen SG, Yang J, Bhavnani SK, *et al*. Analysis of the TGFβ-induced program in primary airway epithelial cells shows essential role of NF-κB/RelA signaling network in type II epithelial mesenchymal transition. *BMC Genomics* 2015;16:529.
19. Bertolusso R, Tian B, Zhao Y, Vergara L, Sabree A, Iwanaszko M, *et al*. Dynamic cross talk model of the epithelial innate immune response to double-stranded RNA stimulation: coordinated dynamics emerging from cell-level noise. *PLoS One* 2014;9: e93396.
20. Brasier AR, Tian B, Jamaluddin M, Kalita MK, Garofalo RP, Lu M. RelA Ser276 phosphorylation-coupled Lys310 acetylation controls transcriptional elongation of inflammatory cytokines in respiratory syncytial virus infection. *J Virol* 2011;85: 11752–11769.
21. Tian B, Zhao Y, Sun H, Zhang Y, Yang J, Brasier AR. BRD4 mediates NF-κB-dependent epithelial-mesenchymal transition and pulmonary fibrosis via transcriptional elongation. *Am J Physiol Lung Cell Mol Physiol* 2016;311:L1183–L1201.
22. Tian B, Yang J, Zhao Y, Ivanciuc T, Sun H, Garofalo RP, *et al*. Bromodomain containing 4 (BRD4) couples NFκB/RelA with airway inflammation and the IRF-RIG-I amplification loop in respiratory syncytial virus infection. *J Virol* 2017;91:pii: e00007-17.
23. Tian B, Liu Z, Yang J, Sun H, Zhao Y, Wakamiya M, *et al*. Selective molecular antagonists of the bronchiolar epithelial NF-κB-bromodomain-containing protein 4 (BRD4) pathway in viral-induced airway inflammation. *Cell Rep* 2018;23:1138–1151.
24. Devaiah BN, Lewis BA, Cherman N, Hewitt MC, Albrecht BK, Robey PG, *et al*. BRD4 is an atypical kinase that phosphorylates serine2 of the RNA polymerase II carboxy-terminal domain. *Proc Natl Acad Sci USA* 2012;109:6927–6932.
25. Devaiah BN, Case-Borden C, Gegonne A, Hsu CH, Chen Q, Meerzaman D, *et al*. BRD4 is a histone acetyltransferase that evicts nucleosomes from chromatin. *Nat Struct Mol Biol* 2016;23: 540–548.
26. Nowak DE, Tian B, Jamaluddin M, Boldogh I, Vergara LA, Choudhary S, *et al*. RelA Ser276 phosphorylation is required for activation of a subset of NF-kappaB-dependent genes by recruiting cyclin-dependent kinase 9/cyclin T1 complexes. *Mol Cell Biol* 2008;28: 3623–3638.
27. Tian B, Patrikeev I, Ochoa L, Vargas G, Belanger KK, Litvinov J, *et al*. NF-κB mediates mesenchymal transition, remodeling and pulmonary fibrosis in response to chronic inflammation by viral RNA patterns. *Am J Respir Cell Mol Biol* 2017;56:506–520.
28. Filippakopoulos P, Qi J, Picaud S, Shen Y, Smith WB, Fedorov O, *et al*. Selective inhibition of BET bromodomains. *Nature* 2010;468: 1067–1073.
29. Picaud S, Wells C, Felletar I, Brotherton D, Martin S, Savitsky P, *et al*. RVX-208, an inhibitor of BET transcriptional regulators with selectivity for the second bromodomain. *Proc Natl Acad Sci USA* 2013;110:19754–19759.
30. Scott GD, Blum ED, Fryer AD, Jacoby DB. Tissue optical clearing, three-dimensional imaging, and computer morphometry in whole mouse lungs and human airways. *Am J Respir Cell Mol Biol* 2014;51: 43–55.
31. Hubner RH, Gitter W, El Mokhtari NE, Mathiak M, Both M, Bolte H, *et al*. Standardized quantification of pulmonary fibrosis in histological samples. *Biotechniques* 2008;44:507–511, 514–517.
32. Brewster CEP, Howarth PH, Djukanovic R, Wilson J, Holgate ST, Roche WR. Myofibroblasts and subepithelial fibrosis in bronchial asthma. *Am J Respir Cell Mol Biol* 1990;3:507–511.
33. Boser SR, Mauad T, Araújo-Paulino BB, Mitchell I, Shrestha G, Chiu A, *et al*. Myofibroblasts are increased in the lung parenchyma in asthma. *PLoS One* 2017;12:e0182378.
34. Evans MJ, Van Winkle LS, Fanucchi MV, Plopper CG. The attenuated fibroblast sheath of the respiratory tract epithelial-mesenchymal trophic unit. *Am J Respir Cell Mol Biol* 1999;21: 655–657.
35. Knight D. Epithelium-fibroblast interactions in response to airway inflammation. *Immunol Cell Biol* 2001;79:160–164.
36. Gizycki MJ, Adelroth E, Rogers AV, O'Byrne PM, Jeffery PK. Myofibroblast involvement in the allergen-induced late response in mild atopic asthma. *Am J Respir Cell Mol Biol* 1997;16:664–673.
37. Zhang S, Smartt H, Holgate ST, Roche WR. Growth factors secreted by bronchial epithelial cells control myofibroblast proliferation: an in vitro co-culture model of airway remodeling in asthma. *Lab Invest* 1999;79:395–405.
38. Bui DS, Burgess JA, Lowe AJ, Perret JL, Lodge CJ, Bui M, *et al*. Childhood lung function predicts adult chronic obstructive pulmonary disease and asthma-chronic obstructive pulmonary disease overlap syndrome. *Am J Respir Crit Care Med* 2017;196:39–46.
39. Stefanowicz D, Ullah J, Lee K, Shaheen F, Olumese E, Fishbane N, *et al*. Epigenetic modifying enzyme expression in asthmatic airway epithelial cells and fibroblasts. *BMC Pulm Med* 2017;17:24.
40. Chang H, Liu Y, Xue M, Liu H, Du S, Zhang L, *et al*. Synergistic action of master transcription factors controls epithelial-to-mesenchymal transition. *Nucleic Acids Res* 2016;44:2514–2527.
41. Liu Z, Wang P, Chen H, Wold EA, Tian B, Brasier AR, *et al*. Drug discovery targeting bromodomain-containing protein 4. *J Med Chem* 2017;60:4533–4558.
42. Brown JD, Lin CY, Duan Q, Griffin G, Federation A, Paranal RM, *et al*. NF-κB directs dynamic super enhancer formation in inflammation and atherogenesis. *Mol Cell* 2014;56:219–231.
43. Zhang Y, Sun H, Zhang J, Brasier AR, Zhao Y. Quantitative assessment of the effects of trypsin digestion methods on affinity purification-mass spectrometry-based protein-protein interaction analysis. *J Proteome Res* 2017;16:3068–3082.
44. Ruscitti F, Ravanetti F, Essers J, Ridwan Y, Belenkov S, Vos W, *et al*. Longitudinal assessment of bleomycin-induced lung fibrosis by micro-CT correlates with histological evaluation in mice. *Multidiscip Respir Med* 2017;12:8.

45. De Langhe E, Vande Velde G, Hostens J, Himmelreich U, Nemery B, Luyten FP, *et al*. Quantification of lung fibrosis and emphysema in mice using automated micro-computed tomography. *PLoS One* 2012;7:e43123.
46. Holgate ST, Holloway J, Wilson S, Bucchieri F, Puddicombe S, Davies DE. Epithelial-mesenchymal communication in the pathogenesis of chronic asthma. *Proc Am Thorac Soc* 2004;1:93–98.
47. Carroll NG, Perry S, Karkhanis A, Harji S, Butt J, James AL, *et al*. The airway longitudinal elastic fiber network and mucosal folding in patients with asthma. *Am J Respir Crit Care Med* 2000;161: 244–248.
48. Karvonen HM, Lehtonen ST, Harju T, Sormunen RT, Lappi-Blanco E, Mäkinen JM, *et al*. Myofibroblast expression in airways and alveoli is affected by smoking and COPD. *Respir Res* 2013;14:84.
49. Kim KK, Kugler MC, Wolters PJ, Robillard L, Galvez MG, Brumwell AN, *et al*. Alveolar epithelial cell mesenchymal transition develops in vivo during pulmonary fibrosis and is regulated by the extracellular matrix. *Proc Natl Acad Sci USA* 2006;103: 13180–13185.
50. Phillips RJ, Burdick MD, Hong K, Lutz MA, Murray LA, Xue YY, *et al*. Circulating fibrocytes traffic to the lungs in response to CXCL12 and mediate fibrosis. *J Clin Invest* 2004;114:438–446.